Journal of Colloid and Interface Science 378 (2012) 201–209

Contents lists available at SciVerse ScienceDirect

Journal of Colloid and Interface Science

www.elsevier.com/locate/jcis

Self-organised microdots formed by dewetting in a highly volatile liquid

Rita Toth [a,*], Jakob Heier [b], Jean-Nicolas Tisserant [b], Enyedy Eva Anna [c], Artur Braun [a], Thomas Graule [a,d]

[a] Laboratory for High Performance Ceramics, Empa. Swiss Federal Laboratories for Materials Science and Technology, CH-8600 Dübendorf, Switzerland
[b] Laboratory for Functional Polymers, Empa. Swiss Federal Laboratories for Materials Science and Technology, CH-8600 Dübendorf, Switzerland
[c] Department of Inorganic and Analytical Chemistry, University of Szeged, H-6701 Szeged, Hungary
[d] Technische Universität Bergakademie Freiberg, D-09599 Freiberg, Germany

ARTICLE INFO

Article history:
Received 24 November 2011
Accepted 3 April 2012
Available online 18 April 2012

Keywords:
Hexagonal and tetragonal order
Dewetting
Self-organisation
Iron oxide microstructure
Microdot
Stick–slip motion
Receding contact line

ABSTRACT

Dewetting induced self-organisation was used to prepare an ordered microstructure from a highly volatile liquid. Dewetting of an evaporating iron oxide precursor solute on silicon substrate resulted in arrays of microdots with nearly hexagonal and tetragonal symmetries. Ordered structures form either by stick–slip motion or fingering instability at the receding contact line of evaporating droplets. Subsequent thermal treatment at 550 °C yields crystalline Fe_2O_3 microdots with a diameter range of 1–4 μm. The size, density and shape of the microdots can be changed by using patterned substrates with different surface energies.

1. Introduction

Synthesising materials with ordered microstructures has attracted increasing interest recently. Functional materials with periodical patterns have a range of applications, for example optical devices, sensors, and photoelectrodes.

The conventional methods to pattern materials are the so called top-down techniques, which are based on fabrication of the material by removing parts of it, i.e. lithography methods. Recently, interest has turned to the so called bottom-up approaches, where the structure is formed from building blocks. Building blocks are typically organic molecules, nanoparticles, etc., which self-assemble or self-organise into larger aggregates induced by intermolecular interactions, e.g. van der Waals forces, electrostatic interactions, hydrogen bonds or hydrophobic effects. Self-assembly is a process driven by the chemical potential towards the thermodynamic equilibrium. Self-organising systems have to be kept far from the equilibrium by continuous supply of matter or energy in order to increase its entropy [1–3].

Solvent evaporation and dewetting are simple, inexpensive, bottom-up surface patterning methods to organise non-volatile materials into ordered microscopic structures. Pattern formation driven by the dewetting of an evaporating solution is a self-organisation process since the entropy of the entire system increases by the heat loss due to the evaporating solvent, even though a part of it, the solute, organises into droplets. Solvent evaporation induced dewetting can lead to the formation of micrometer-sized droplets [4]. Solvent evaporation methods based on a moving three-phase contact line have been employed to form ordered structures of materials ranging from small organic molecules [4,5] and polymers [6–9] to nanocrystalline salts, nanorods and nanoparticles [10–12]. Various models were developed to reproduce several aspects of the experimental findings [13–15]. The recession of the contact line, i.e. the edge of an evaporating liquid drop on a solid substrate, can also be non-continuous, causing a so called stick–slip motion, i.e. fast receding is followed by "pinning" [5,6,14]. At each stick–slip step, regularly spaced droplets or stripes parallel to the contact line are deposited on the substrate where the contact line was pinned. The pattern consists of droplets or lines, depending on the type [6] and the concentration of the employed materials [5]. Since dewetting is a general phenomenon of liquids, many different materials can be used: polymers [9,16,17], dye-containing polymers [18,19], nanoparticles [20], and small organic molecules in liquid phase [21]. It has also been shown that fluctuations in the solute concentration close to the contact line leads to a fingering instability [8,9,13]. The fingers recede more slowly on the substrate due to their higher concentration, i.e. higher viscosity. Therefore the fingers elongate, destabilise and break up into droplets similarly to the Plateau-Rayleigh instability found in liquid jets. In this way a 2D ordered pattern forms.

* Corresponding author.
E-mail address: Rita.Toth@empa.ch (R. Toth).

0021-9797/$ - see front matter © 2012 Elsevier Inc. All rights reserved.
http://dx.doi.org/10.1016/j.jcis.2012.04.011

In this paper we describe ordered iron oxide microdots with patterns reminiscent to hexagonal and tetragonal symmetry in a highly volatile iron oxide precursor solution. Pattern formation due to the receding contact line of a drop of polymer or macromolecule solution, or nanoparticle suspension has been intensively studied using single-drop deposition or dip-coating methods. Whereas spin coating as depositing technique has not been widely exploited yet for experiments with receding contact lines. During spin coating the thickness of a thin film of a volatile liquid is continuously reduced not only by evaporation but also by spinning. This combined effect can be the source of a wide variety of patterns. Here we spin coat a dilute macromolecule solution on silicon wafers. The two major processes governing the pattern formation at different stages of the spin coating process are contact line pinning and fingering instability. The receding contact lines of the drops, formed at the early stage of spin coating, shows stick–slip motion, as well as fingering instabilities. The parameters affecting the size and the order of the microdots have been investigated. The effect of the spin coating solvents has also been studied. The size, density and shape of the microdots were altered by using substrates with a pattern of different surface energies. The pattern that is obtained after spin coating consists of the solid iron oxide precursor and probably some remnant solvent. The precursor pattern is transformed to crystalline hematite pattern by following the patterning by pyrolysis at 550 °C [22].

2. Materials and methods

2.1. Materials

Iron(III)acetylacetonate (99%) and benzoylacetone (99%) were purchased from Acros Organics and Aldrich Chemicals, respectively. Methanol (gradient grade, >99.8% (GC) for HPLC) and chloroform (anhydrous, ⩾99%) were purchased from Fluka and Sigma–Aldrich, respectively. 0.45 μm, 17 mm Titan HPLC–PTFE filter membranes were purchased from Infochroma AG, Switzerland. Silicon wafers (p ⟨ 1 0 0 ⟩ >, with native oxide layer) were purchased from Si-Mat, Germany. The wafers were cleaned in acetone in an ultrasonic bath, then rinsed with ethanol and dried with compressed nitrogen. Chromium and gold pellets for metal deposition were purchased from CERAC Inc., USA. The base and curing agent for poly(dimethylsiloxane) (PDMS, Sylgard 184-Dow Corning) stamps and heptadecane-1-thiol were purchased from Troller Kunststoffe AG, Switzerland and Sigma Aldrich, respectively.

2.2. Solution preparation

The solution preparation is based on the recipe described in [23] substituting titanium butoxide with iron(III)acetylacetonate (Fe(acac)). Fe(acac) and benzoylacetone (bzac) were mixed in 1 ml methanol and stirred for 2 h at ambient temperature. To this precursor solution 3 ml chloroform (or 1-pentanol) was added and stirred for a further 15 min to produce a dilute solution for spin coating. The solution was filtered and then 0.1 ml was spin coated onto a 1×1 cm^2 piece of silicon wafer.

Iron(III) complexes formed with the bidentate ligands acac and bzac have similar stoichiometry (MA^{2+}, MA_2^+, MA_3) and stability on the basis of literature data [24], however, complexes of bzac represent slightly higher stability. The original form of the $[Fe(acac)_3]$ may be varied by changing its analytical (total) concentration, the acac-to-bzac ratio and the solvent; and species such as $[Fe(acac)_2]^+$, $[Fe(acac)(bzac)]^+$ can form and may become major species (for more information see Supplementary data, S2). While in the nonpolar chloroform solvent the neutral complexes, such as $[Fe(acac)_3]$, $[Fe(acac)_2(bzac)]$, $[Fe(acac)(bzac)_2]$ are probably more favourable, in polar solvents, such as alcohols, the $[Fe(acac)_2]^+$, $[Fe(acac)(bzac)]^+$ complexes may form more readily.

2.3. Spin coating

In order to prepare a thin film by spin coating a dilute solution is placed on a substrate and subjected to rotation. The spin coating process involves three stages. In the first stage, the solution spreads on the substrate and most of it is spun off due to the centrifugal force. After the first stage, a thin layer of solution remains on the substrate. In the second stage, this layer gets thinner as a result of liquid flow. The rapid evaporation of the solvent increases the viscosity of the solution and slows the shear thinning of the film. The pattern formation occurs in this stage. In the third stage, the solvent evaporation conserves the developed pattern. Generally, the structures are created in a nonequilibrium stage, resulting from the rapid solvent quench, since typical spin coating times are only 30–60 s. Due to the rapid solvent quench, the patterns solidify during spin coating and the final pattern is the dried solute (with some residual solvent).

The films were spin coated in two steps with low acceleration. In the first step 500 rpm was reached with 100 rpm/s acceleration in 5 s (spreading and hydrodynamic thinning phase). In the second step the spin coater was accelerated with 300 rpm/s to 4000 rpm (evaporative thinning). The second spin speed was varied between 2000 and 6000 rpm.

2.4. Characterisation

Images were recorded using an optical microscope (Leica) attached to a camera.

A thermographic camera (model: Cedip Jade III MWIR, from Cedip Infrared Systems, SAS, (now FLIR), France) was used to follow the temperature change during spin coating.

Laser reflectometry (laser diode from ILEE, Switzerland (www.ilee.ch), model V35MV1, lambda = 750 nm) was used to determine the initial thickness of the film prior to evaporation and to follow the thickness evolution over time [25].

The grazing incidence X-ray diffraction (GIXRD) spectra have been taken with a Siemens D5000 diffractometer with Cu K(α1) wavelength source. The incidence angle was fixed at 3° for the entire measurement and the diffraction signals were collected from 20 to 80°.

3. Results

When a solution of equimolar amounts (50 mM final concentration each) of Fe(acac) and bzac dissolved in chloroform is spin coated onto silicon wafers, highly ordered microdots form. Some areas have nearly hexagonal, others tetragonal symmetry (Fig. 1). The diameter of the dots varies between 1.4 and 4 μm and the distances between them is 2.6–10 μm, depending on the experimental parameters (discussed later). The height of the microdots is around 100–200 nm. Quantitative analysis of the AFM height profile of a representative area with dots (Fig. 1b) yields an average dot height of 110 nm ± 17.5 nm and a full width at half maximum (FWHM) of 1.61 μm. The centres of the dots are separated by 6.1 μm from each other. Fig. 1b shows the profile fitted with a series of Gaussians with 1.61 μ FWHM and separation of 6.1 μ. Fig. 2 shows the temperature transient during spin coating, obtained by a thermographic camera. Infrared radiation of a 2 mm × 2 mm area in the middle of the substrate is measured. The measured infrared radiation is corrected by the emissivity of the substrate (0.8) in order to obtain the true temperature transient. In the first 3–4 s the film and substrate cool down to a minimum temperature and in

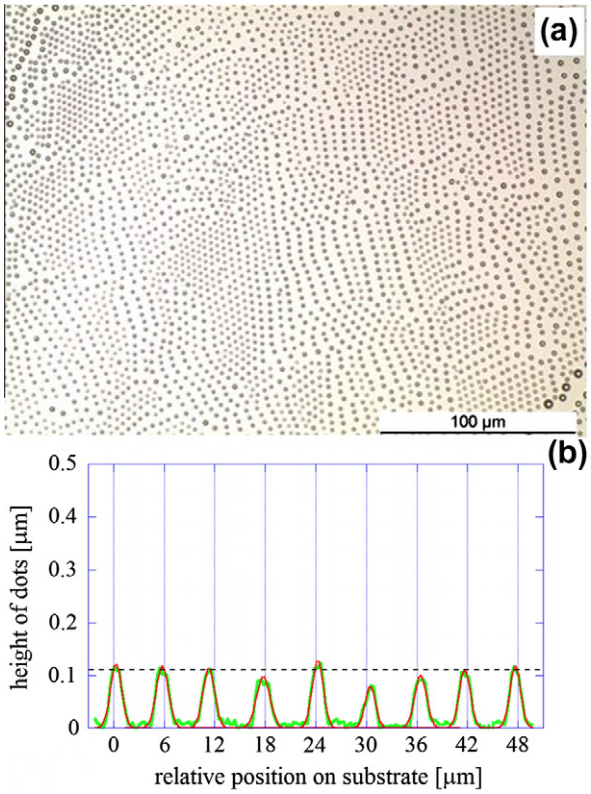

Fig. 1. (a) Optical micrograph of a typical area of ordered patterns of solute microdots dried during spin coating a solution of Fe(acac) and bzac mixture (50 mM each) in chloroform (4000 rpm spin coating speed). (b) Height profile (open symbols) of a representative row of dots fitted (solid line) with a sequence of Gaussians note that the axes are anisometric.

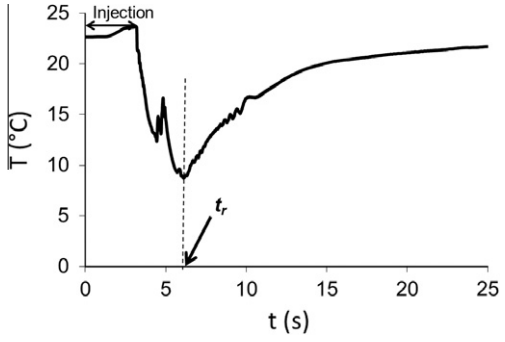

Fig. 2. Typical temperature transient of the film and substrate during spin coating a solution of Fe(acac) and bzac mixture (50 mM each) in chloroform (4000 rpm spin coating speed) obtained with a thermographic camera. The first ~3 s correspond to the injection of the liquid onto the substrate. After injection the temperature decreases rapidly for about 3 s and then increases slowly to ambient temperature. The lowest temperature is assumed to correspond to the time t_r when the film ruptures.

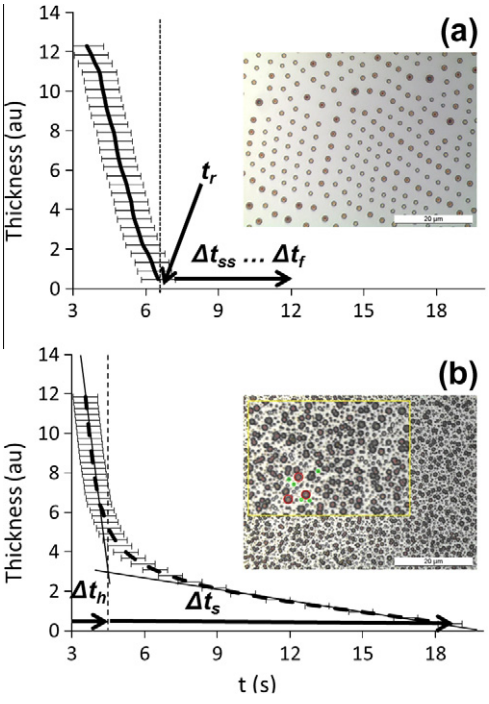

Fig. 3. The evolution of the thickness of a 0.1 ml drop of Fe(acac)–bzac solution (50 mM each) with spin coating solvents (a) chloroform and (b) 1-pentanol during spin coating (4000 rpm) determined with laser reflectivity measurement. Note that below 3.5 s the measurement is not possible because of the limited time resolution of our instrument. (a) Ordered pattern forms and the thickness changes linearly with a steep slope; t_r is proposed to be the time when the film suddenly ruptures and large drops form. The contact lines of the formed drops recedes with stick–slip motion (Δt_{ss}) and droplets parallel to the contact lines form. Later, microdots form with fingering instability (Δt_f). Δt_{ss} andΔ t_f cannot be determined with laser reflectivity with our setup. (b) The size distribution is bimodal as first larger dots form (red in inset) with heterogeneous dewetting (Δt_h), then spinodal dewetting (Δt_s) results in smaller dots (green in inset) (data from [4]). The scale bars are 20 µm.

the subsequent ~20 s they warm up to ambient temperature. This indicates that most of the solvent evaporates during the acceleration step (first 5 s) of the spin coating process.

The initial thickness of the film is around 10 µm; as it was determined by the specular reflectivity of a laser beam pointing at the film during spin coating [25]. Because the pattern formation occurs during spin coating, it was not possible to study this process visually in real time. However, we monitored the thickness evolution of the films during spin coating, using the aforementioned laser reflectivity measurement (Fig. 3). Two different solutions were spin coated; one containing chloroform (Fig. 3a), and the other 1-pentanol as spin coating solvent (Fig. 3b). For the former, the thickness decreases with a constant speed, as is revealed by the linear decrease in Fig. 3a. For the latter we observe a nonlinear decrease of the film thickness. The formed pattern is ordered with unimodal size distribution (Fig. 6) when the spin coating solvent is chloroform and disordered with bimodal size distribution when the spin coating solvent is 1-pentanol (data for 1-pentanol are from [4], a previous publication of the authors). We assume that the time (t_r) after which no further thickness change can be detected, corresponds to an abrupt film rupture in Fig. 3a. This rupture prevents the formation of a thin evaporating film responsible for the tail of the curve in Fig. 3b. It is noteworthy to mention that the same t_r is found on the temperature transient curve in Fig. 2. This means that most of the solvents evaporate in the first 3 s, corresponding to the spreading and hydrodynamic thinning phase of spin coating, after which the system slowly warms up to ambient temperature. The evaporation of the remnant solvent causes the small kinks on the curve after t_r (Fig. 2). It is shown in [4 and references therein] that two consecutive mechanisms result in a bimodal size distribution when 1-pentanol is used as spin coating solvent (Fig. 3b): the larger dots form initially by heterogeneous dewetting of the thicker film and the smaller dots form by spinodal dewetting of the very thin film remaining between the large dots. We postulate that the initial steep part of the curve (spreading and hydrodynamic thinning phase of spin coating) corresponds to droplet formation by heterogeneous dewetting (Δt_h) and the tail of the curve (evaporative thinning phase) corresponds to spinodal dewetting (Δt_s) of the

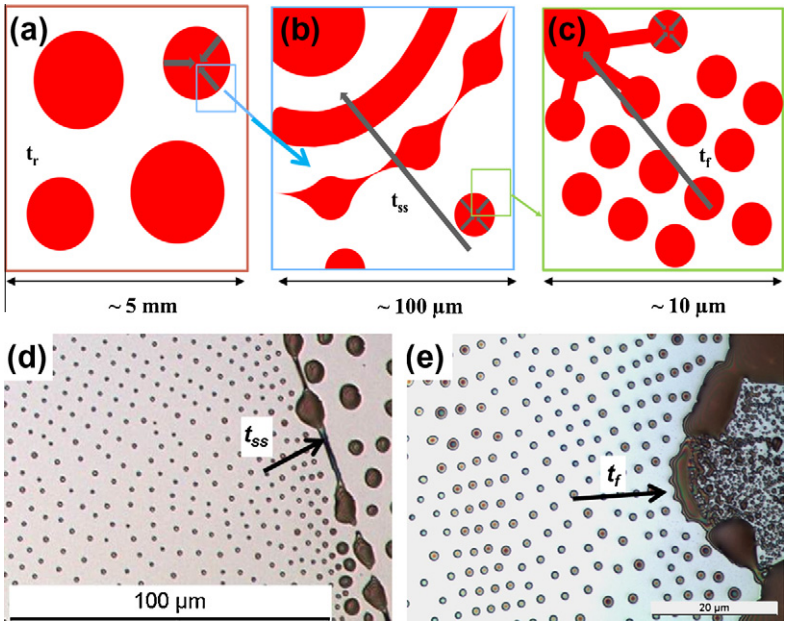

Fig. 4. (a–c) Schematic representation of the pattern formation processes. (a) The rupture of the film at t_r results in large drops of the solution (mm range). (b) The contact line of the drops recedes with stick–slip motion (Δt_{ss}), resulting in periodic stripes. The stripes then break into droplets by Rayleigh instability. (c) The receding contact line of some of the droplets is destabilised by fingering instability (Δt_f) resulting in ordered microdots. (d and e) are experimental images of (b and c) respectively (Fe(acac)–bzac mixture (17 mM each), chloroform solvent and 4000 rpm spin coating speed).

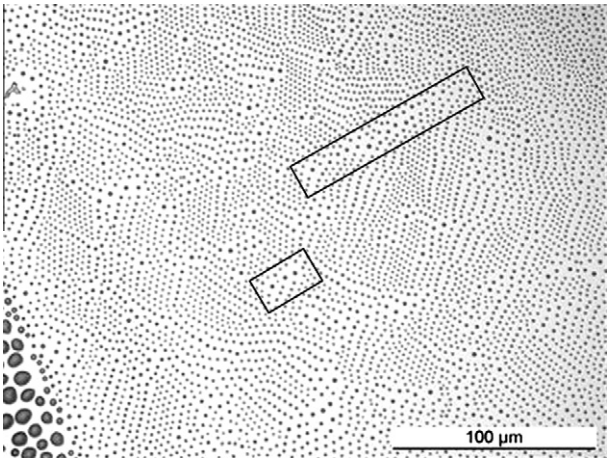

Fig. 5. Larger microdots between ordered areas are typically indicative to collision lines of microdots (some examples are framed). Fe(acac)–bzac mixture (33 and 25 mM, respectively), chloroform solvent and 4000 rpm spin coating speed.

very thin film remained between the droplets. The formation of rather large (mm range diameter) droplets of the Fe(acac) and bzac solution when spin coated from chloroform (Fig. 3a) remains a question of debate. Differently from the solutions cast from 1-pentanol, no evaporative thinning phase is detected with the laser reflectometer. This suggests that the film fully ruptures in an early stage (at t_r) into very large domains. This cannot be explained from the surface energies of the solvent; we believe that viscous forces or forces due to fast solvent evaporation prevent the formation of a continuous liquid film already in an early stage.

The next stage of the process is related to the recession of the contact line of the formed drops while the remnant solvent evaporates.

Droplets of different size and volume originate from different evaporation rates, the pattern therefore is composed of areas where different stages of the pattern formation are "dried in" at the end of the spin coating (Fig. 4d and e). These patterns let us speculate about the mechanism of the pattern formation. For example, to explain the patterns in Fig. 4d and we postulate the following mechanisms: after the rupture of the film (Fig. 4a) the remaining solvent evaporates and the contact line of the large drops recede with stick–slip motion or develop fingering instability. Each time the contact line is pinned to the substrate, a stripe of solution deposits which then ruptures into droplets due to Rayleigh instability (Fig. 4b, schematic representation). The arrow shows the evolution of the pattern over time during the stick–slip motion (Δt_{ss}) and the direction of the recession. The contact lines may also develop fingering instability. In the fingers or undulations the concentration of the solute is higher than in the regions in between [5,6,13,15], therefore that part of the contact line recede more slowly, develop a bottleneck and finally disintegrate into ordered dots driven by Rayleigh instability. A hypothesised evolution of the pattern over time by fingering instability (Δt_f) is shown in Fig. 4c with an arrow indicating the direction of the recession of the contact line. In Fig. 4d an arrow shows the dried in stage of a stripe of solution breaking up into droplets. This is indicative of the stick–slip motion of the contact line, which is therefore responsible for the formation of the larger droplets (5–10 µm diameter) in Fig. 4d (right side). The smaller dots (1–2 µm) on the left side of the image may have formed by fingering instability of the contact line of the large droplets. Fig. 4e clearly shows a dried in stage of an undulated contact line (arrow) which indicates that the small dots on the left side of the image formed by fingering instability.

These results are in qualitative agreement with the theoretical results presented in Fig. 12 of [13]. In [13] pattern formation from a drop of suspension due to evaporation of the solvent is modelled using Dynamical Density Functional Theory. The authors found that as the dewetting front recedes it collects colloids, therefore the concentration of the colloids increases near the front (the concentration of the solute increases close to the contact line in our case) and at a certain threshold density value the liquid near the front separates into two phases, a mobile one with less colloids, and a less mobile one with more colloids (higher and lower concentration of the solute in our experiments). This effect results in

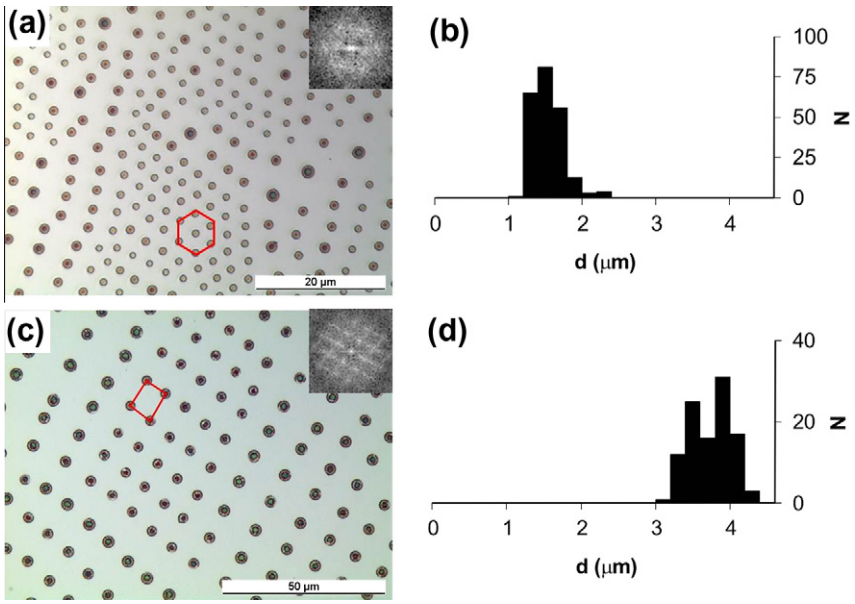

Fig. 6. Optical micrographs of ordered patterns of Fe(acac) and bzac mixture (50 mM each) in chloroform. (a) Hexagonal order with 4000 rpm spin coating speed. The inset is the Fourier transform of the figure, (b) size distribution of (a), *N*: number of dots on the selected area, (c) rectangular order of the same iron oxide precursor microdots using 2000 rpm spin casting speed. The inset is the Fourier transform of the figure, (d) size distribution of (c), *N*: number of dots on the selected area.

fingering instability and a branched structure forms. From the areas where the colloid density is higher, thicker fingers (branches) form, and from the areas where the colloid density is lower, very thin fingers develop which quickly rupture into a series of droplets. As the interaction energy between the colloids increases, the number of the fingers increases, and finally all the fingers are replaced by droplets. One could speculate that in our experiments initially the receding contact line contains more solvent, consequently, the concentration of the solute is lower, which results in thin fingers ruptured into small droplets (left side of Fig. 4d). As the solvent evaporates, the concentration of the solute increases near the contact line, thicker fingers develop and rupture into larger droplets. This could also be the reason for the much bigger droplet size on the right side of Fig. 4d and also in the lower left corner of Fig. 5.

Since the microdots develop from a curved contact line they form numerous areas of ordered dots, each with different orientation, instead of one large area. When a row of dots, formed from a curved contact line, collides with a row of microdots from a curved contact line with a tilt to the opposite direction, a "collision line" develops (Fig. 5). Similar collision lines were observed with polystyrene microdots in [9]. Typically, microdots in collision lines are larger than the surrounding dots. There are several collision lines along the receding contact line and after the complete recession a very complex pattern is formed. The boundaries between the areas with different symmetries within the pattern potentially are caused by the grain boundaries in the silicon wafer.

3.1. Size dependence

The size of the microdots and the distance between them can be controlled by the spin-coating speed. At higher spin coating speeds smaller dots develop closer together. The mean diameter of microdots is 1.4 (4) μm with 2.6–3.1 (8–10) μm distances between them for 4000 rpm (2000 rpm) spin coating speeds (Fig. 6). The Fast Fourier transform (FFT) images show tetragonal (2000 rpm) and hexagonal symmetries (4000 rpm).

3.2. Parameters affecting the ordering

3.2.1. Concentration of Fe(acac) and bzac

The ordering of the microdots is affected by the concentration of Fe(acac) and bzac. There is a narrow range of concentrations where ordered patterns form (Fig. 7). Ordered patterns are present on the largest area of the substrate inside the framed area in Fig. 7. When the concentration of one of the two reactants is very low (below 12 mM) rings form instead of dots. Rings and long chain like microstructures also form when the Fe(acac) concentration is relatively high, i.e. 50 mM compared to bzac concentration (12–30 mM and 12–42 mM, respectively), see Supplementary information S1. The molecular weight of Fe(acac) is more than twice that of bzac and its density is five times higher. Therefore, increasing the Fe(acac) concentration increases the viscosity of the solution more significantly than increasing the bzac concentration. The form of the $[Fe(acac)_3]$ depends on its analytical (total) concentration and the acac-to-bzac ratio (see Supplementary information S2) and species such as $[Fe(acac)_2]^+$ and $[Fe(acac)(bzac)]^+$ can form and may become major species. These forms of the complex change the polar part of the surface energy of the solution and, consequently, effect the spreading of the solution. The ordering in the pattern is driven

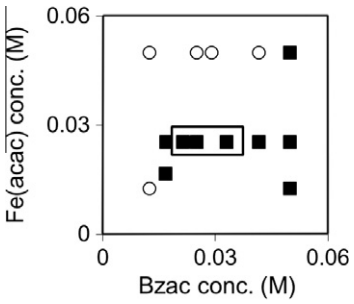

Fig. 7. The effect of Fe(acac) and bzac concentrations on the pattern formation. ■: ordered, ○: unordered structures with 4000 rpm spin-coating speed and chloroform as the spin coating solvent.

by the nonlinear dependence of the viscosity on the concentration [14] and a result of an intricate balance of viscosity, surface tension, and solid–liquid interactions.

3.2.2. Solvent evaporation rate

3.2.2.1. Spin coating speed. The spin coating speed for one specific solvent also affects the ordering of the microdots via the speed of evaporation. There is an optimal spin-coating speed (~4000 rpm) at which ordered structures form in the largest concentration range. At lower and higher than optimal speed ordered microdots form in a much smaller concentration range. At high spin coating speed the film thickness changes rapidly and there is no time for the ordered structure to form with stick–slip motion or fingering instability. Above the critical film thickness (low spin coating speed) the film stabilising forces (gravity and surface tension) start to dominate.

The results of the concentration and spin coating speed dependences can be qualitatively compared with the results of a dynamical model in [14]. Regular line formation, caused by contact line recession of a suspension drop, is modelled and a morphological phase diagram is presented in the function of evaporation number (which can be related to our spin coating speed) and bulk concentration in Fig. 3 in [14]. In agreement with our results they also found that there is only a certain parameter range where an ordered pattern (regular stripes) is found.

It is not surprising that we found ordered patterns only at a narrow range of parameters considering that self-organising systems have nonlinear dynamics. All nonlinear systems are very sensitive to the initial parameters; small variations can have a drastic effect on the final structure [3,26]. The self-organised cycles of "sticking" and "slipping" of the contact line is driven by the strong nonlinear dependence of the viscosity on the concentration, in an intricate interaction with evaporation and diffusion; as it has been shown in a theoretical work in [14].

3.2.2.2. Solvent. Although the solvent in this paper was not changed we can study the solvent effect on ordering by using the data from our previous work [4], where the evaporation rate of the same precursor solution was varied by changing the solvent. Since, apart from the solvent, all the experimental parameters were the same we can compare the results of the two papers. When less volatile solvents (for example methanol, ethanol, 1-pentanol, 2-octanol) are used instead of chloroform in [4], no ordered pattern is found for the concentration and spin coating parameter ranges we studied with chloroform (Fig. 8). The evaporation rate of the solution with chloroform is around 13–19 μl/s, while with ethanol it is around 5–6 μl/s (Fig. 3). The evaporation rates were estimated from laser reflectometry data; the time when the thickness stops decreasing (most of the solvent has evaporated) can be determined and the initial volume of the injected solution is known (the surface area of the substrates is the same). These estimations do not give the correct value for the evaporation rate, as the initial spin-off of the solution during the first stage of spin coating is not considered. These values are only an indication that the solution with chloroform solvent evaporated over three times faster than with ethanol, which is in good agreement with the vapour pressure of the solvents (p_c = 21.15 kPa and p_e = 5.83 kPa at 20 °C). Also, while a unimodal size distribution was observed with more volatile solvents, i.e. chloroform and methanol, the size distribution was bimodal with less volatile solvents such as ethanol, 1-pentanol and 2-octanol. We showed in [4] that the bimodal size distribution is a result of different dewetting mechanisms at different film thicknesses during spin coating. Heterogeneous dewetting is responsible for the formation of dots at higher thicknesses, and spinodal dewetting breaks up the thin film into smaller, densely packed dots at lower thicknesses (see Ref. [4]). With the more volatile methanol the film reaches the critical thickness for spinodal dewetting very quickly, therefore, heterogeneous nucleation cannot set on and the size distribution is unimodal. With chloroform the size distribution is also unimodal but the mean dot size of the ordered dots is smaller (0.7 and 1.2 μm radius for chloroform and methanol, respectively) and the distance between them is much greater then with methanol (2.6–3.1 and 0–1.2 μm for chloroform and methanol, respectively, for the same spin coating speed), i.e. the coverage (the percentage of the area of the image that is covered by dots) is much less (Fig. 8). This difference in the coverage (i.e. the dot size and the distance between them) and the different symmetry of the patterns support our proposition that the mechanism of the ordered pattern formation is not spinodal dewetting.

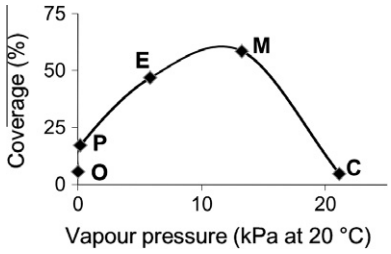

Fig. 8. Effect of decreasing solvent volatility on coverage. Coverage (%) = area of the dots (μm^2)/area of the whole image (μm^2) × 100. C: chloroform, M: methanol, E: ethanol, P: 1-pentanol, O: 2-octanol. Note: data for M, E, P and O were taken from [9]. (Fe(acac) and bzac concentrations: 50 mM each, spin coating speed 4000 rpm.)

To further explore the effect of the solvents we placed microdrops of pure solvents and Fe(acac)–bzac solutions with different solvents on a silicon wafer from a micropipette and observed the spreading and the contact angle of the micro-drops. Comparing the surface energies of the solvents (chloroform 27.16, methanol 22.7, ethanol 21.97, 1-pentanol 25.36 mN/m) to a silicon wafer with native oxide layer (89 mN/m) all solvents should wet the surface. Indeed, all of the solvents and solutions partially wet the silicon wafer, i.e. their contact angles are less than 90° and increase from methanol to octanol for the alcohols. The chloroform's contact angle was similar to the octanol's, however, the chloroform evaporated much faster. The contact line of the solvent microdrops pinned to the substrate and left a solid ring behind. However, only the chloroform pinned repeatedly, forming a solid target pattern. The solutions behaved the same way; only the contact line of the solution micro-drop with chloroform pinned periodically to the surface. This observation supports our suggested mechanism because the same periodic pinning-depinning (stick slip motion) can also happen with the drops formed at the early stage of spin coating. Another indication of our mechanism is that the alcohols are polar, while the chloroform is nonpolar; therefore the polar solid–liquid interactions are strong between the alcohols and the hydrophilic silicon wafer and the alcohols dewet the silicon wafer when the film thicknesses are low (third stage of spin-coating). As the solid–liquid interaction is weaker (the contact angle is larger) between the chloroform and the silicon wafer, the chloroform dewets the silicon wafer at high thicknesses (at the first or second stage of spin coating), resulting in large drops. The contact line of these drops then recedes with stick slip motion forming periodic lines and droplets.

When the concentrations of Fe(acac) and bzac are high, the solution spread slightly better than the pure chloroform. The possible reason is the presence of the $[Fe(acac)_2]^+$, $[Fe(acac)(bzac)]^+$ ions in the solution which make the solution slightly more polar.

3.3. Order on pre-structured surfaces

To overcome the size limitation and material restriction of lithography techniques some methods combine lithography and

Table 1
Spin coating parameters.

Time (s)	Acceleration (rpm/s)	Spin speed (rpm)
5	100	500
30	300	2000–6000

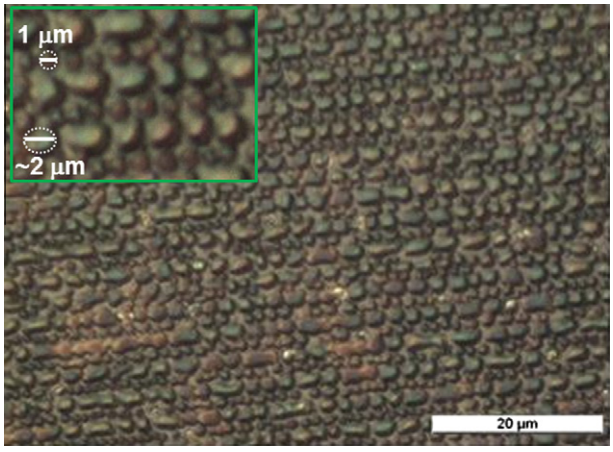

Fig. 9. Micrograph of the directed order of the microdots on patterned substrate prepared by micro-contact printing. The order of the dots follows the pattern of the substrate. (Fe(acac) and bzac concentrations: 50 mM each, spin coating solvent chloroform and spin coating speed 4000 rpm.)

dewetting, i.e. use selective wetting or dewetting on prestructured substrates. The structure of the substrate comprises areas with different surface energies, and is typically a hydrophilic/hydrophobic pattern prepared by photolithography or micro contact printing. Because dewetting depends on the interfacial energies, the material selectively wets or dewets the different surfaces. Patterning can induce novel morphologies in the film emerging from additional degrees of freedom [27].

We managed to direct the order of the microdots and to decrease the distance between them significantly by using prestructured substrates. The surface tension of the substrate was locally changed using the micro-contact printing technique. Thiol-bearing molecules are known to bind strongly onto gold surfaces and to form a so-called thiol self-assembled monolayer (SAM) [28–30]. A 3 nm thick chromium layer and a 30 nm thick gold layer were deposited on glass by low pressure metal deposition. The typical deposition rate was 0.1 Å s^{-1} with a starting pressure of 6×10^{-6} mbar. A patterned poly(dimethylsiloxane) (PDMS) stamp was prepared by pouring a vacuum degassed 10:1 (wt:wt) base:curing agent mixture onto a pre-patterned silicon wafer. The stamp was cured at ambient temperature for 24 h. This PDMS stamp was used to control the size and position of these SAMs on gold surface. The stamp was swelled by heptadecane-1-thiol solution (1 M or 0.5 M) in ethanol and upon contact between the stamp and the gold surface diffusion transfers the thiol molecules only at the contact area. The result was a periodic pattern of 1 μm wide gold and 2 μm wide SAM stripes. A solution of equimolar amounts (0.05 mM each) of Fe(acac) and bzac dissolved in chloroform was spin coated onto the patterned surface (See spin coating parameters in Table 1.) and underwent lateral phase separation. Periodic stripes of dots formed following the pattern of the substrate (Fig. 9) instead of the intrinsic ordered pattern. On the gold stripes ~1 μm diameter, and on the SAM stripes ~2 μm diameter dots formed. The size of the 1 μm dots and the distance between them (0.2–0.75 μm) significantly smaller compared with the spontaneously ordered dots. This method provides a potential way of tailoring the size, density and shape of the dots.

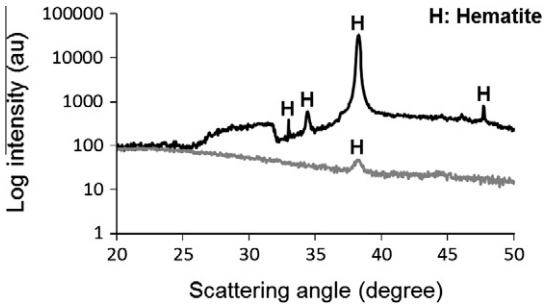

Fig. 10. GIXRD patterns of the annealed microdots on glass (grey diffractogram, bottom) and gold (black diffractogram, top) substrate. The hematite phase was identified. (See details of the measurement in Section 2.4.) The microdots were prepared by spin coating (4000 rpm) an Fe(acac)–bzac mixture (50 mM each) using chloroform as spin coating solvent.

While in polymer systems the competition between the natural instability length scale and the imposed length scale of the pattern typically leads to very specific conditions under which pattern replication can be achieved [31–35], we here demonstrate that in our case the imposed pattern sets the dimensions of the generated structures. That is another indication for our proposed mechanisms. While in the "regular" experiments, the contact lines are free to move, here they are pinned to the border between plain substrate and SAM.

3.4. Structures after annealing

After deposition the structures were annealed at 550 °C in air to oxidise the dried iron containing solute to crystalline hematite. The samples were placed on a covered corundum boat and were annealed in an electric furnace with the following temperature program: the samples were heated to 400 °C with heating rate: 4.44 K/min and were kept at 400 °C for 30 min. Then the temperature was increased to 550 °C with heating rate: 2.5 K/min and it was kept at 550 °C for 90 min. Finally the samples were cooled down to ambient temperature with cooling rate: approx. 2.9 K/min. After annealing only iron oxide in hematite form remained on the surface of the substrate. The deep red[1] colour of the Fe(acac) turned into the brownish-red colour of hematite. The hematite phase was identified by GIXRD measurements (see details of the measurement in Section 2.4) (Fig. 10). In [22,22a] it was shown by thermogravimetric and X-ray diffraction analysis that the annealing temperature has an important role in achieving the desired iron oxide phase for thin films prepared by metal organic deposition from Fe(acac). When the films are annealed at 400 °C the crystalline γ-Fe_2O_3 (maghemite) phase forms. However, at higher temperatures the metastable γ-Fe_2O_3 transforms into the polycrystalline α-Fe_2O_3 phase. The AFM images (not shown) before and after annealing show that the structure and symmetry is preserved. The diameter of the microdots does not change, whereas their height decreases significantly.

4. Conclusions

In this paper we show that ordered microdots with nearly hexagonal and tetragonal symmetry form in a highly volatile solution of an iron oxide precursor, i.e. Fe(III)acetylacetonate, during spin coating with low acceleration and speed. Firstly the film ruptures and large drops form. Stick–slip motion and fingering instability of the contact line results in ordered microdots with nearly

[1] For interpretation of colour in Figs. 1,3,4,6 and 9, the reader is referred to the web version of this article.

hexagonal and tetragonal symmetries. The size and distance between the microdots is decreased by increasing the spin coating speed. Ordered patterns form at a rather narrow range of parameters. There is an optimal spin coating speed for ordered pattern formation, below and above which the ordering decreases significantly. Ordered pattern is present on the largest area at a small concentration range of Fe(acac) and bzac.

We have studied the effect of solvent on the ordering in greater detail comparing the present results (using chloroform) with our previous data from [4], where various alcohols were used as spin coating solvents. We found that the type of solvent affects the ordering: ordered microdots were only found with chloroform, while solvents methanol, ethanol, 1-pentanol and 2-octanol resulted in irregular microdots [4]. Moreover, using more volatile solvents as spin coating solvent, i.e. chloroform and methanol, resulted in a unimodal size distribution, while with less volatile solvents, such as ethanol, 1-pentanol and 2-octanol, bimodal size distribution was found. We showed in [4] that the bimodal size distribution is a result of two different dewetting mechanisms at different film thicknesses during spin coating (heterogeneous dewetting at higher thicknesses and spinodal dewetting at lower thicknesses) and the unimodal size distribution with methanol was caused by spinodal dewetting alone. In this paper, using chloroform as spin coating solvent, also unimodal size distribution has been found. However, the mean dot size for the ordered dots with chloroform is much smaller, and the distance between the dots is much greater than for methanol. This difference in the dot size and in the distance between the dots, together with the difference in the symmetry (ordered and unordered) of the patterns suggest that the ordered pattern formation with chloroform is not a result of spinodal dewetting. When micro-drops of the above discussed solvents and solutions made with these solvents were placed on silicon wafers, only the pure chloroform and the solution made with chloroform formed solid concentric rings on the silicon wafer during solvent evaporation, due to the periodically pinning contact line (stick slip motion) of the drop. This supports our mechanism that the contact lines of the drops, formed at an early stage of spin coating of an Fe(acac)–bzac solution made with chloroform, recede with stick slip motion. The main difference between the solvents is that the alcohols are polar, while the chloroform is nonpolar, therefore the polar solid–liquid interactions are stronger between the alcohols and the hydrophilic silicon wafer and the alcohols dewet the silicon wafer only when the film thicknesses are low (third stage of spin-coating). As the solid–liquid interactions are weaker (the contact angle is larger) between the chloroform and the silicon wafer, the chloroform dewets the silicon wafer at higher thicknesses (first or second stage of spin coating), resulting in large drops. The contact lines of these drops then recede with stick slip motion forming periodic lines and droplets. Fingering instability of the contact line also develops, resulting in smaller dots. Since fingering instability is typical at the dewetting front of ultra-thin layers [37,13], in our case fingers presumably form at a later stage, when the thickness is reduced due to solvent evaporation.

The size, density and shape of the microstructure were altered by using substrates with a pattern of different surface energies. The ordering of the periodic microdots is commensurate with the pattern of the microcontact printed substrate. While in polymer systems the competition between the natural instability length scale and the imposed length scale of the pattern typically leads to very specific conditions, in our case the imposed pattern sets the dimensions of the generated structures, because the contact lines are pinned to the border between plain substrate and SAM. That is another indication for our proposed mechanisms.

The hexagonal or tetragonal ordering could potentially be scaled up by sliding two substrates on top of each other, a method described in [5] with polymers. The achieved pattern can be controlled by the sliding speed and the concentration of the polymer/macromolecules.

Metal acetylacetonates are general precursors for the synthesis of metal oxide nanoparticles [36]. Fe(III)acetylacetonate is a precursor for hematite nanoparticle preparation [38,39]. Hematite is an inexpensive photoactive material, which can be used in photovoltaic applications. It has been suggested that in such applications patterning can improve the performance of the photoelectrodes [40] or the presented ordered circular shapes could potentially be useful for organic light emitting diode applications [21].

Acknowledgments

Financial support for R.T. by the Empa Board of Directors 7th R&D Program and by the European Union FP7 Project “Nanostructured Photoelectrodes for Energy Conversion (NanoPEC)”, Novel Materials for Energy Applications (Grant No. 227179) is gratefully acknowledged. The authors thank Erwin Hack and Roman Furrer for the IR- and Tzu-Wen Huang for the XRD measurement. During finalisation of the manuscript R.T. was financially supported by the Marie Heim-Vögtlin (MHV) Grant (No. PMPDP2-139689/1).

Appendix A. Supplementary material

Supplementary data associated with this article can be found, in the online version, at http://dx.doi.org/10.1016/j.jcis.2012.04.011.

References

[1] A.L.R. Jones, Soft Machines: Nanotechnology and Life, Oxford University Press, 2004.
[2] K. John, M. Bär, Phys. Rev. Lett. 95 (2005) 198101.
[3] R.C. Desai, R. Kapral, Dynamics of Self-Organized and Self-Assembled Structures, Cambridge University Press, 2009.
[4] R. Toth, M. Schabikowski, J. Heier, A. Braun, D. Kata, T. Graule, J. Mater. Res. 26 (2011) 1.
[5] R.v. Hameren, P. Schon, A.M.v. Buul, J. Hoogboom, S.V. Lazarenko, J.W. Gerritsen, H. Engelkamp, P.C.M. Christianen, H.A. Heus, J.C. Maan, T. Rasing, S. Speller, A.E. Rowan, J. Elemans, R.J.M. Nolte, Science 314 (2006) 1433.
[6] R.Z. Rogowski, A.A. Darhuber, Langmuir 26 (2010) 11485.
[7] W. Sele, B.K.C. Kjellander, B. Niesen, M.J. Thornton, J.v.d. Putten, K. Myny, H.J. Wondergem, A. Moser, R. Resel, A.v. Breemen, N.v. Aerle, P. Heremans, J.E. Anthony, G.H. Gelinck, Adv. Mater. 21 (2009) 4926.
[8] H. Yabu, M. Shimomura, Adv. Function. Mater. 15 (2005) 575.
[9] O. Karthaus, L. Grasjo, N. Maruyama, M. Shimomura, Chaos 9 (1999) 308.
[10] J.H. Wu, B. Varghese, X.D. Zhou, S.Y. Teo, C.H. Sow, S.G. Ang, G.Q. Xu, Chem. Mater. 22 (2010) 1533–1539;
J.H. Wu, S.G. Ang, G.Q. Xu, J. Phys. Chem. C 112 (2008) 7605–7610.
[11] Z.X. Deng, C.D. Mao, Langmuir 20 (2004) 8078–8082.
[12] Z.X. Wang, T. Kong, K. Zhang, H.L. Hu, X.P. Wang, J.G. Hou, J. Chen, Mater. Lett. 61 (2007) 251–255.
[13] M.J. Robbins, A.J. Archer, U. Thiele, J. Phys.: Condens. Matter 23 (2011) 415102.
[14] L. Frastia, A.J. Archer, U. Thiele, Phys. Rev. Lett. 106 (2011) 077801.
[15] I. Vancea, U. Thiele, E. Pauliac-Vaujour, A. Stannard, C.P. Martin, M.O. Blunt, P.J. Moriarty, Phys. Rev. E 78 (2008) 041601.
[16] S.W. Hong, J. Xu, Z.Q. Lin, Nano Lett. 6 (2006) 2949.
[17] O. Karthaus, K. Ijiro, M. Shimomura, Chem. Lett. 9 (1996) 821.
[18] O. Karthaus, K. Okamoto, R. Chiba, K. Kaga, Intl. J. Nanosci. 1 (2002) 461.
[19] O. Karthaus, T. Imai, J. Sato, S. Kurimura, R. Nakamura, Appl. Phys. A 80 (2005) 903.
[20] J. Huang, F. Kim, A.R. Tao, S. Connor, P. Yang, Nat. Mater. 4 (2005) 896.
[21] O. Karthaus, C. Adachi, S. Kurimura, T. Oyamada, Appl. Phys. Lett. 84 (2004) 4696.
[22] B. Pal, M. Sharon, Thin Solid Film 379 (2000) 83.
[23] N.E. Voicu, M.S.M. Saifullah, K.R.V. Subramanian, M.E. Welland, U. Steiner, Soft Matter 3 (2007) 554.
[24] S.J. End et al., Inorg. Chim. Acta 278 (1978) 170–177.
[25] P.C. Jukes, S.Y. Heriot, J.S. Sharp, R.A.L. Jones, Macromolecules 38 (2005) 2030.
[26] I.R. Epstein, J.A. Pojman, An Introduction to Nonlinear Chemical Dynamics: Oscillations, Waves, Patterns, and Chaos, Oxford University Press, 1998.
[27] P. Lenz, R. Lipowsky, Phys. Rev. Lett. 80 (1998) 1920.
[28] A. Kumar, G.M. Whitesides, Appl. Phys. Lett. 63 (1993) 2002.
[29] J.C. Love, L.A. Estroff, J.K. Kriebel, R.G. Nuzzo, G.M. Whitesides, Chem. Rev. 105 (2005) 1103.
[30] J.E. ten Elshof, S.U. Khan, O.F. Göbel, J. Eur. Ceram. Soc. 30 (2010) 1555.
[31] A. Karim, J.F. Douglas, B.P. Lee, S.C. Glotzer, J.A. Rogers, E.J. Amis, G.M. Whitesides, Phys. Rev. E: Stat. Phys. Plasmas, Fluids, Relat. Interdiscip. Top. 57 (1998) R6273–R6276.

[32] M. Boltau, S. Walheim, J. Mlynek, G. Krausch, U. Steiner, Nature 391 (1998) 877–879.
[33] L. Rockford, Y. Liu, P. Mansky, T.P. Russell, M. Yoon, S.G.J. Mochrie, Phys. Rev. Lett. 82 (1999) 2602–2605.
[34] B.D. Ermi, G. Nisato, J.F. Douglas, J.A. Rogers, A. Karim, Phys. Rev. Lett. 81 (1998) 3900–3903.
[35] G. Nisato, B.D. Ermi, J.F. Douglas, A. Karim, Macromolecules 32 (1999) 2356–2364.
[36] A.L. Willis, Z. Chen, J. He, Y. Zhu, N.J. Turro, S. O'Brien, J. Nanomater. 2007 (2007) 1–7 (Article ID 14858).
[37] E. Pauliac-Vaujour, P. Moriarty, J. Phys. Chem. C 111 (2007) 16255.
[38] V.M. Bogatyrev, V.M. Gun'ko, M.V. Galaburda, M.V. Borysenko, V.A. Pokrovskiy, O.I. Oranska, E.V. Polshin, O.M. Korduban, R. Leboda, J. Skubiszewska-Zie, J. Colloid Interface Sci. 338 (2009) 376.
[39] H. Kominami, S.-i. Onoue, K. Matsuo, Y. Kera, J. Am. Ceram. Soc. 82 (1999) 1937.
[40] B.M. Kayes, H.A. Atwater, N.S. Lewis, J. Appl. Phys. 97 (2005) 114302.